Digest Journal of Nanomaterials and Biostructures Vol. 19, No. 3, July -September 2024, p. 1129 - 1146

Preparation and characterization of Ea-AgNPs-Si nanocomposite: investigating it as a poultry reformer, pathogen suppressor, sprouting catalyst and adsorbent

D. Gnanasangeetha[a,*], K. Kannan[b]
[a]*Department of Chemistry, PSNA College of Engineering & Technology, Dindigul – 624 622, TN, India*
[b]*Department of Mechanical Engineering and Advanced Institute of Manufacturing with High-Tech Innovations, National Chung Cheng University, Chiayi County, 621301, Taiwan*

This study synthesizes nano composite (Ea-AgNPs-Si) using Euphorbia antisyphilitica(Ea), employing it as a poultry reformer, sorptive material, pathogen suppressor and sprouting catalyst. Characterization involved XRD, SEM, TEM, Zetasizer, UV-Visible and FT-IR techniques. Ea-AgNPs-Si adopted a face centered cubic arrangement with average crystalline size of 20.34 nm. Zeta potential assessed stability. PDI value of Ea-AgNPs-Si nanocomposite is 1 indicating the polydisperse distribution. SEM revealed flower shape (Ea-AgNPs-Si), ranging 70-100 nm in diameter. The disc diffusion method reveals that Ea-AgNPs-Si exhibits potent antimicrobial activity at 60 µl against Staphylococcus aureus, Actinomycetes, Escherichia coli, Klebsiella pneumonia and Pseudomonas aeruginosa, attributed to its deep diffusion and release of silver ions and silica. It is unequivocally evident from the data that Langmuir isotherm and Pseudo II order model provides a superior fit approaching R^2 value as 0.9972, 0.9461, 0.916, 0.9827, 0.9455 and 0.9534 for LA(I), LA(II), LA(III) describing monolayer chemisorption onto surfaces with uniform adsorption energies than Freundlich, Tempkin and BET models, which is synonymous with the results obtained from R2011a Matlab neuro solution. Through final germination (FG) we concluded that among 130 corriandrum seeds sown,109 sprouted in 20 days. Higher germination index (GI) T2>T4>T1>T3> expedited that Ea-AgNPs-Si shall be used as a nutrient to boost the growth of crops. Ordinarily, it necessitates a span of 45 days for a single batch to attain harvest readiness; however, through our efforts, we have accomplished this feat in a mere 20 days. Henceforth, Ea-AgNPs-Si shall be employed as a Poultry Reformer, Pathogen Suppressor, Sprouting Catalyst and Adsorbent.

(Received May 18, 2024; Accepted July 31, 2024)

Keywords: Euphorbia antisyphilitica, Nano composite, Adsorbent, Germination index, Liquid ammonia

1. Introduction

Nanoparticles, ranging from 1 to 100 nanometers, offer unique properties due to their high surface/volume ratio, quantum effects and surface energy. They find applications across medicine, electronics, environmental science and materials engineering. In medicine, they promise targeted drug delivery, imaging and therapeutics. In electronics, they enhance device efficiency. In environmental science, they aid in pollution remediation and energy conversion. Their unique properties promote escalation. Green synthesis methods aim to produce nanoparticles using environmental friendly approaches. Techniques like plant-mediated synthesis, microbial synthesis, biopolymer-assisted synthesis, microwave-assisted synthesis and solar-assisted synthesis utilize natural sources or renewable energy (1-5). These methods reduce the environmental footprint of nanoparticle synthesis promoting sustainability. Silver nanoparticles (AgNPs) find extensive applications owed to their antimicrobial, electric, catalytic and optic properties. They serve as antimicrobial agents in medical products, facilitate drug delivery in biomedical applications and are

* Corresponding author: sangithprakash@yahoo.in
https://doi.org/10.15251/DJNB.2024.193.1129

incorporated into textiles for odour prevention. AgNPs also enhance conductivity in electronics, catalyse reactions and purify water in environmental applications. Additionally, they're used in cosmetics and food packaging to prevent microbial contamination and extend shelf life. These applications demonstrate the versatility and significance of silver nanoparticles across various industries. Overall silver nanoparticles represent a frontier in materials science with vast potential to revolutionize industries. *Euphorbia antisyphilitica(Ea)*, known as the Candelilla plant, is a perennial succulent native to the Chihuahuan Desert region, primarily found in Texas, New Mexico and northeastern Mexico. Belonging to the Euphorbiaceae family, it's recognized for succulent stems and unique growth habits. Candelilla plant forms clumps of slender, erect stems, reaching 1 to 2 feet in height, with a waxy coating giving them a candle-like appearance. Its reduced, scale-like leaves aid in water conservation, while small, inconspicuous flowers cluster in terminal inflorescences called cyathia. Adapted to arid environments, *E. antisyphilitica* thrives in sandy or rocky soils, commonly found in desert scrublands and rocky slopes. It plays a vital ecological role by providing habitat and food for desert wildlife, attracting pollinators and aiding seed dispersal. Culturally, indigenous tribes historically utilized the plant for medicinal and cultural purposes, extracting wax for candles and medicinal ointments. Today, Candelilla wax is commercially harvested for cosmetics, pharmaceuticals and other industries. Overall, *Euphorbia antisyphilitica* stands as a remarkable desert succulent, showcasing unique adaptations and cultural significance within desert ecosystems (6-10). As for we know, there are no reported studies on the synthesis of silver nanoparticles (AgNPs) using *Euphorbia antisyphilitica*. Reported silver nanoparticles on various herbs is listed in Table 1.

Table 1. Reported silver nanoparticles on various herbs.

S. No.	Plant Species	Family	Reported NPs appox.	Shape	Phytoconstituents	Reference
1.	*Lantana*	Verbenaceae	34	Spherical	Secondary Metabolites	[11]
2.	*Swallowwort*	Asclepiadaceae	50	FCC	Polysaccharides	[12]
3.	*Brazilian fleabane*	Asteraceae	---	Globular	Caffeic acid derivatives	[13]
4.	*Bitter melon*	Cucurbitaceae	10.9	Spheroidal	Momordin	[14]
5.	*Indian mulberry*	Rubiaceae	100	Rod	Nutrients & Micronutrients	[15]
6.	*Black seed*	Ranunculaceae	14-15	Globular	Antioxidants	[16]
7.	*Giant salvinia*	Salviniaceae	12	Spheroidal	Biomolecules	[17]
8.	*Betle leaf*	Piperaceae	47.9-82.9	Spherical	Aminocarboxylic acids	[18]
9.	*Aloe vera*	Asphodelaceae	---	Spheroidal	Lignin, hemicellulose and pectins	[19]
10.	*Wormwood*	Asteraceae	19.9	Round	Hydroxybenzenes	[20]
11.	*Mountain ebony*	Fabaceae	31.9	Ten-sided polygon	Reducing sugars	[21]
12.	*Bracken fern*	Dennstaedtiaceae	34.8	Globular	Phenols, alkaloids, tannins, flavonoids, proteins, carbohydrates, saponins. glycosides, steroids and triterpenoids	[22]
13.	*Japanese cherry*	Rosaceae	---	Spheroidal	Polypeptides	[23]
14.	*Pennyroyal* sp.	Lamiaceae	19	Globular	Phenylpropenes	[24]

S. No.	Plant Species	Family	Reported NPs appox.	Shape	Phytoconstituents	Reference
15.	*Neem*	Meliaceae	35.7	Spheroidal	Oxygenated derivatives of terpenes	[25]
16.	*Vasaka*	Acanthaceae	9.7	Spherical	Adhatodine	[26]
17.	*West African Locust*	Fabaceae	24.7	Globular	Prolamins	[27]
18.	*Dutchman's Pipe*	Aristolochiaceae	31.5	Circular	Aristolochic acid	[28]
19.	*Grapevine*	Vitaceae	199.9	Spheric	Kaempferol and gallic acid	[29]
20.	*Night shade*	Solanaceae	50	Round	Phenolic compounds	[30]
21.	*Indian Cucumber*	Cucurbitaceae	---	Orb-like	Hydroxy benzenes	[31]
22.	*Rio Grande amaranth*	Amaranthaceae	13	Polycrystalline	Aminoalkanoic acids	[32]
23.	*Jerusalem sage*	Lamiaceae	25	Rounded	Glycosides such as flavonoids, iridoids, diterpenoids, triterpenoids and other phenolic compounds	[33]
24.	*Blue gum*	Myrtaceae	4	---	Eucalyptine	[34]
25.	*Indian Pennywort*	Apiaceae	20.9	Globular	Asiaticoside	[35]
26.	*Teak*	Lamiaceae	27	Spheric	Caffeic acid	[36]
27.	*Indian mahogany*	Meliaceae	19	Round	Amide-I and amide-II	[37]
28.	*Balloon vine*	Sapindaceae	99	Ball	Polyphenols and phenol	[38]
29.	*Tooth cup*	Lythraceae	--	Circular	Rutin & ferulic acid	[39]
30.	*Paradise Tree*	Simaroubaceae	48	Spheric	Isoleucine &Phenylalanine	[40]
31.	*Sweet marjoram*	Lamiaceae &	39	Rounded	Proteins and phenolic compounds	[41]
32.	*Guava*	Myrtaceae	87	Orb-like	Leucocyanidin, vitamin C& B6	[42]
33.	Tropical Water Willow	Acanthaceae	19	Rounded	Quercetin	[43]
34.	*Yellow Skimmia*	Rutaceae	--	Six-sided	Lupeol & Oleanolic acid	[44]
35.	*False Water willow*	Acanthaceae	69	Cubical	Emodin & Rhein	[45]
36.	*Child Life Tree*	Putranjivaceae	6	Spherical	Argenine & Lysine	[46]
37.	*European ash*	Oleaceae	---	Multi-disperse	Aspartic acid & Glutamic acid	[47]
38.	*Indian Beech*	Fabaceae	---	Spherical	Alkaloids, glycosides, flavonoids, saponins, carbohydrates, tannins, phenolic compounds and fat	[48]

S. No.	Plant Species	Family	Reported NPs appox.	Shape	Phytoconstituents	Reference
39.	*Indian birthwort*	Aristolochiaceae	55	Cubical	Phenols	[49]
40.	*Indian laburnum*	Fabaceae	31.6	Triangular	sennosides A and B	[50]
41.	*Indian coleus*	Lamiaceae	34	Spheric	Rosemarinic acid	[51]
42.	*Slender amaranth*	Amaranthaceae	19	----	Hexanal	[52]
43.	*Damson plum*	Sapotaceae	24.6	Flower	Olivifosides	[53]
44.	*Saraca indica*	Fabaceae	22.9	Round	Flavonoids and steroids	[54]
45.	*Gokhru*	Pedaliaceae	49.8	Ball	Apigenin	[55]
46.	*Talbot's fig*	Moraceae	11	Globular	Stanols	[56]
47.	*Country mallow*	Malvaceae	29	Prism	Leptosins	[57]
48.	*Blue Glory*	Lamiaceae	14	Spherical	Luteolin	[58]
49.	*Thwaites' Ceropegia*	Apocynaceae	9	Spheric	Betulinic acid	[59]
50.	*Dwarf Copperleaf*	Amaranthaceae	29	Various shape	Dietary fibre, sugar& starch	[60]
51.	*Candelilla*	Euphorbiaceae	20.34	Flower	Octacosanol & triacontanol	Current Material

2. Materials and methods

2.1. Preparation of extract

All the chemicals used were of analytic grade (Sigma Aldrich, 99%). Euphorbia antisyphilitica(Ea) specimens were sourced from a private farm, followed by drying and pulverization using a grinder. To create an aqueous extract (10% w/v), 10 g of the powder were mixed with 100 ml of deionized water in a 500 ml Erlenmeyer flask, heated to 50°C on a hot plate for 1 hour. The extract was obtained by centrifuging the mixture at 2000 rpm for 10 minutes, filtering through a Buchner funnel with Whatman no. 1 paper, and stored the filtrates in a refrigerator.

2.2. Synthesis of AgNPs

0.01697g AgNO3 dissolved in 100 ml distilled water to produce 1mM solution of AgNO3. To separate 10 mL portions of the AgNO3 solution of 1mM, different amounts of Ea extract (1 ml, 2 ml, 3 ml, 4 ml and 5 ml) were added and kept silver nitrate concentration the same at 1 mM. Ea-AgNPs was synthesized by changing the concentration of AgNO3, ranging from 1 mM to 5 mM, keeping the plant extract volume constant at 1 ml and stirred for 2 hrs. This whole setup was placed in a dark room for 12 hrs to prevent light from affecting it and was kept at room temperature. The solution changed colour from clear to brown more effectively in the later one indicating Ag+ions turned into Ag0ions confirms the formation of Ea-AgNPs.

2.3. Synthesis of Ea-AgNPs-Si nano composite

In one beaker, 4.7 grams of TEOS (Tetraethyl orthosilicate) and 8.68 grams of ethanol were added. This mix is called the "alkoxide solution." In another beaker, we added 7.0 millilitres of water to 8.68 grams of ethanol. Then, we added 8-10 drops, of a special solution made of ammonium fluoride and ammonium hydroxide. When TEOS reacts with water, it makes a solution that has a lot of tiny particles of silicic acid. These particles then come together to make even tinier silica particles, each smaller than 5 nanometers. These tiny particles are not very stable and can stick together to become bigger particles. However, they have some charge on their surface that prevents them from sticking together too much. Now, we added 1-7mL in portions Ea-AgNPs into this mixture and stirred for 2 hrs, excess silica particles, encase Ea-AgNPs forming Ea-AgNPs-Si nano-composite.

2.4. Characterisation of Ea-AgNPs-Si

UV-Visible spectral analysis was determined by Shimadzu UV-visible spectrophotometer (model UV-1800), with 1 nm resolution scanning from 200 to 800 nm after samples were diluted in water. FT-IR spectra were recorded on a Perkin Elmer 1750 FTIR spectrophotometer. Scanning electron microscopy (SEM) and energy dispersive X-ray (EDX) were employed for particle size and surface morphology analysis. XRD patterns were obtained using a Rigaku Miniflex 600 X-ray diffractometer (40 kV, 15 mA, Cu Kα radiation, 2θ range 20–80°). Dynamic light scattering (DLS) was determined using Malvern Zetasizer nanosizer for zeta potential and particle size analysis (0.1 to 10,000 nm range).

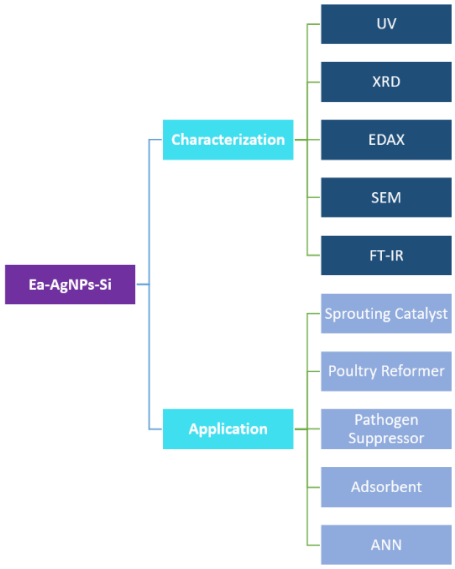

Fig. 1. Characterisation of Ea-AgNPs-Si.

2.5. Antimicrobial assay

Antimicrobial efficacy was assessed via agar diffusion method. Sterile paper discs, each measuring 5 mm in diameter, were soaked with Ea-AgNPs-Si and double-distilled water (used as a control). These discs were then positioned on each plate and subjected to incubation at 36.9°C for 2 days. The antibacterial efficacy was determined by measuring the inhibition zone surrounding the disc containing Ea-AgNPs-Si. The bactericidal potency of Ag nanoparticles, originating from Ea-AgNPs-Si, owes itself to their significant surface/volume ratio and minuscule dimensions, enabling intimate interaction with microbial membranes. The study encompassed an array of pathogenic bacteria, comprising gram +ve strains like Staphylococcus aureus and Actinomycetes sp., alongside gram -ve counterparts like Escherichia coli , Klebsiella p neumonia and Pseudomonas aeruginosa.

2.6. Synthesis of liquid ammonia (LA)

Poultry waste, which contains ammonia in various forms such as uric acid, is collected from poultry farms. The collected waste is mixed with water to form a solution. In preliminary screening solid particles and large debris are removed. The solution is then introduced into a distillation apparatus. This typically consists of a heating element, a distillation vessel, such as a pot and a condenser. The waste solution is heated, causing the ammonia and water vapor to rise as steam. The temperature is carefully controlled to avoid excessive decomposition of ammonia and other undesirable reactions. As the steam rises, it carries with it ammonia and water vapor. The distillation vessel is designed to allow separation of these vapours from other components present in the solution. The steam containing the ammonia and water vapor is then passed through a condenser, where it is cooled and condensed back into a liquid. This condensate contains concentrated ammonia. The condensed liquid, which now contains concentrated ammonia, is collected in a

separate flask is labelled as liquid ammonia (LA) After distillation, the remaining waste solution contains reduced levels of ammonia. This solution is further processed as earlier, until desired purity of the recovered ammonia appears.

2.7. Adsorption isotherm and kinetics

Optimizing adsorption system design requires understanding adsorbate-adsorbent interactions through adsorption isotherms. Equations like Langmuir, Freundlich, Tempkin, BET, Pseudo I and II order to determine parameters reflecting adsorbent surface properties and affinity, aiding system performance optimization. The Freundlich equation empirically models multilayer sorption on heterogeneous surfaces. It is expressed as log qe = log KF + 1/n log Ce, where qe (mg/g) and Ce(mg/L) represent the adsorbed amount and concentration at equilibrium, respectively. The parameters KF and 1/n are determined from the plot of log qe versus log Ce. Langmuir isotherm is valuable for predicting adsorption capacities and understanding mass transfer relationships. It can be expressed as Ce/qe = (1/KL) + (aL/KL) Ce, where KL(L/g) is the Langmuir equilibrium constant and aL/KL represents the theoretical monolayer saturation capacity. The Langmuir parameters are obtained from linear correlations between Ce/qe and Ce. The Langmuir equation generally applies to adsorption on fully homogeneous surfaces. The Tempkin isotherm characterizes adsorption on heterogeneous surfaces, typically expressed as qe = B lnA + B lnCe. By plotting qe versus ln Ce, the constants A and B can be determined. BET method was used to determine the sample's specific surface area, pore volume and pore size by performing N2 adsorption-desorption at -195.629 °C. The pseudo first-order equation ln(qe - qt) = ln qe - k1t describes As(III), Cu(II) and Pb(II) adsorption, with qt and qe as amounts at time t and equilibrium. The rate constant k1 reflects the pseudo first-order rate constant and a linear graph of ln (qe - qt) versus t confirms first-order kinetics. The chemisorption kinetic rate equation is given by t/qt = (1/k2qe2) + (1/qe)t, where k2 is the equilibrium rate constant of the pseudo second-order equation. The linearity of t/qt versus t indicates the best fit with pseudo-second-order kinetics. The empirical data concerning the adsorption of LA(I), LA(II) and LA(III) onto Ea-AgNPs-Si composite underwent rigorous calibration against an array of kinetic models. This examination encompassed a gamut of experimental parameters, spanning initial concentrations of 0.005 to 0.10(mg/L), contact durations ranging from 10 to 120 minutes, pH levels extending from the acidic confines of 1 to the alkaline realm of 12, adsorbent quantities fluctuating between 0.5 and 6 grams and agitation velocities of 50 to 500 revolutions per minute.

2.8. Electrophoretic mobility

The correlation between the surface charge Ea-AgNPs-Si of and their stability is a matter of paramount importance. In order to ascertain the surface charge and the polydisperse distribution of Ea-AgNPs-Si composite, we employed the formidable Malvern-Zeta-sizer (Version 6.32). Furthermore, electrophoretic micrograph was acquired from the same.

2.9. Calculation of germination index (GI)

The germination period (GP) was figured out by counting the days from when the first germination was seen (FG) until no more germination was noticed (NMG). In simple terms, we calculate GP by subtracting FG from NMG. The germination percentage (GC) was calculated by comparing the total seeds sprouted (TGS) to the total seeds sowed (TSS) and then multiplying the result by 100. So, the formula for GC is:

$$GC = (TGS/TSS) \times 100.$$

The germination value (GV) was calculated using a formula:

$$GV = (\sum DGs/N) \times (GP/10).$$ Here's what each part means:

GV is the germination value.GP is the germination percentage at the end of the test. DGs is the daily germination speed, which is found by dividing the total germination percentage by the number of days since planting. N represents the number of daily counts, starting from the day when

the first germination was seen. The number 10 remains constant. So, in simple terms, GV is a value we figure out by considering how quickly the seeds germinated each day. The mean germination rate MGR = (Total number of seeds sprouted on each day) divided by (Total number of days it took for the seeds to germinate). In simpler terms, it's a way to find out how quickly the seeds sprouted on average by looking at the total number of seeds that sprouted each day and how long it took for them to do so. Final germination (FG) was calculated using this formula: FG = (Number of seeds that sprouted when no more were sprouting) divided by (Sum of days it took for those specific seeds to sprout). The germination index (GI) was calculated using this formula: GI = (The total number of seeds that sprouted on each day, denoted as Gt) divided by (The total number of days it took for those seeds to sprout, represented by Dt). Elevated GI values serve as an indicator of more substantial and expedited germination. This formula was adapted by Esechi in 1994. The definition of a favourable outcome in one scientific inquiry may not necessarily align with that in another and this discrepancy is heavily contingent upon the particular data analysis approach applied.

3. Results and discussion

3.1. Characterization of Ea-AgNPs-Si

The existence of silver and silica in Ea-AgNPs-Si was confirmed through a rigorous spectral investigation of visible wavelength spectrum from 200 nm to 800 nm documented in Figure 2. The resultant Ea-AgNPs-Si unveiled a salient and defining feature: the s plasmonic resonance (SPR) band that is emblematic of silver and silica are, precisely centered within the wavelength range of 418 to 440 nm. Notably absence of any discernible peaks is a conspicuous indicator of the utter lack of aggregation. As the concentration of Ea-AgNPs-Si increased, it imparted a greater abundance of biomolecules, thereby significantly augmenting the efficacy of the metal reduction process. The sharpness of the UV-VIS absorption peak at 297 and 440 nm exhibited a direct relationship with the concentration ratio of Ea-AgNPs-Si composite.

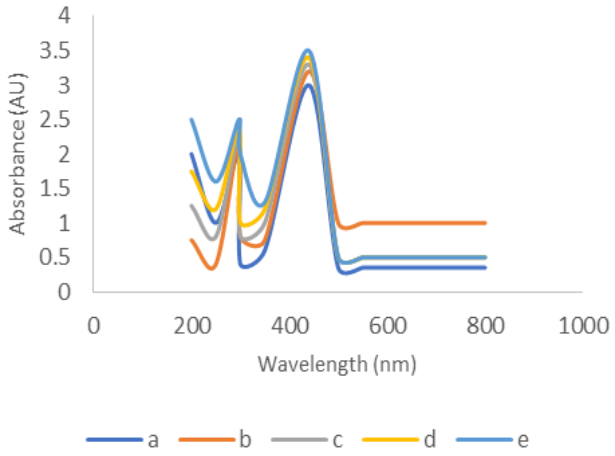

Fig. 2. UV spectra of Ea-AgNPs -Si a) 0.1%, b) 0.2%, c) 0.3 %, d) 0.4 % e) 0.5 % of Ea-AgNPs -Si

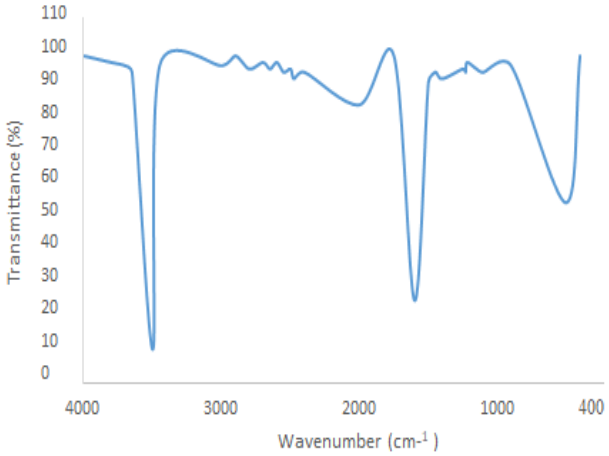

Fig. 3 .FT-IR spectrum of Ea-AgNPs-Si.

The FTIR spectrum of the Ea-AgNPs-Si reveals a multitude of absorption peaks, as depicted in the figure 3. Absorption bands residing within the range of 3500 to 3400 cm^{-1} are attributed to the intermolecular -OH stretching of cresol and -NH stretching of Aniline. The absorption peak at 2924 cm^{-1} are a consequence of cyclohexane stretching vibrations, whereas those at 1664 cm^{-1} stem from the vigorous stretching of C=O bonds in conjugated ketones. Diminished bands within the spectral intervals of 3000-2800 and 1600-1400 cm^{-1} suggest the presence of functional groups facilitating the reduction of silver nanoparticles. Broad peak from 400-1900 cm^{-1} range is due to the stretching vibrations of Si-O-Si. Through FTIR analysis, it is unequivocally established that both (-OH) and amine (-N-H) functional groups play a pivotal role in the reduction of Ag^{+} ions to Ag^{0}. In addition peak at 400cm^{-1} confirms the presence of AgNPs.

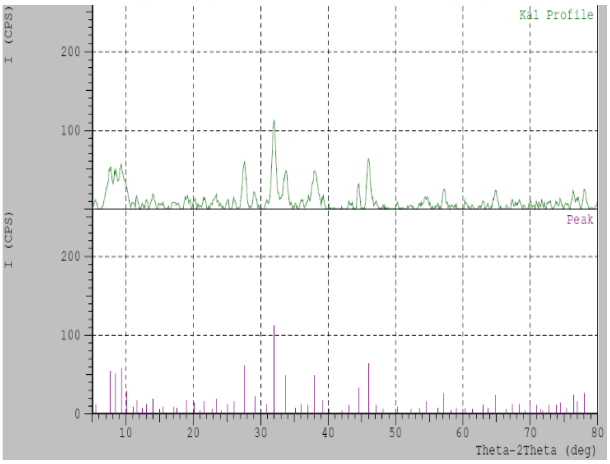

Fig. 4. XRD spectrum of Ea-AgNPs-Si.

In XRD analysis, distinct diffraction peaks were observed at 26,31.97, 38.02,46,65.07 and 78.89 degrees. Comparison of these peaks with established standards revealed that the nanocomposite possessed a crystalline nature. Furthermore, these peaks (100), (101), (111), (200) and (311) facets were attributed to the silver and silica crystal lattice, indicating that composite adopted a face-centered cubic(fcc) arrangement. This finding aligned with data from JCPDS cards (04-0783 and 46-1045). The nanocomposite's average size was determined using Scherrer's equation.

$$D = 0.9 \lambda / \beta \cos \theta$$

where 'λ' representing the wavelength of X-Ray (0.1541 nm), 'β' indicating the FWHM (full width at half maximum), 'θ' representing the diffraction angle and 'D' signifying the size of the particle diameter. Average grain size of the synthesized nanoparticles was found to be 20.34 nm. It's worth noting that the unassigned peaks observed could potentially arise from the crystallization of the bioorganic phase that occurs on the surface of the nanocomposite.

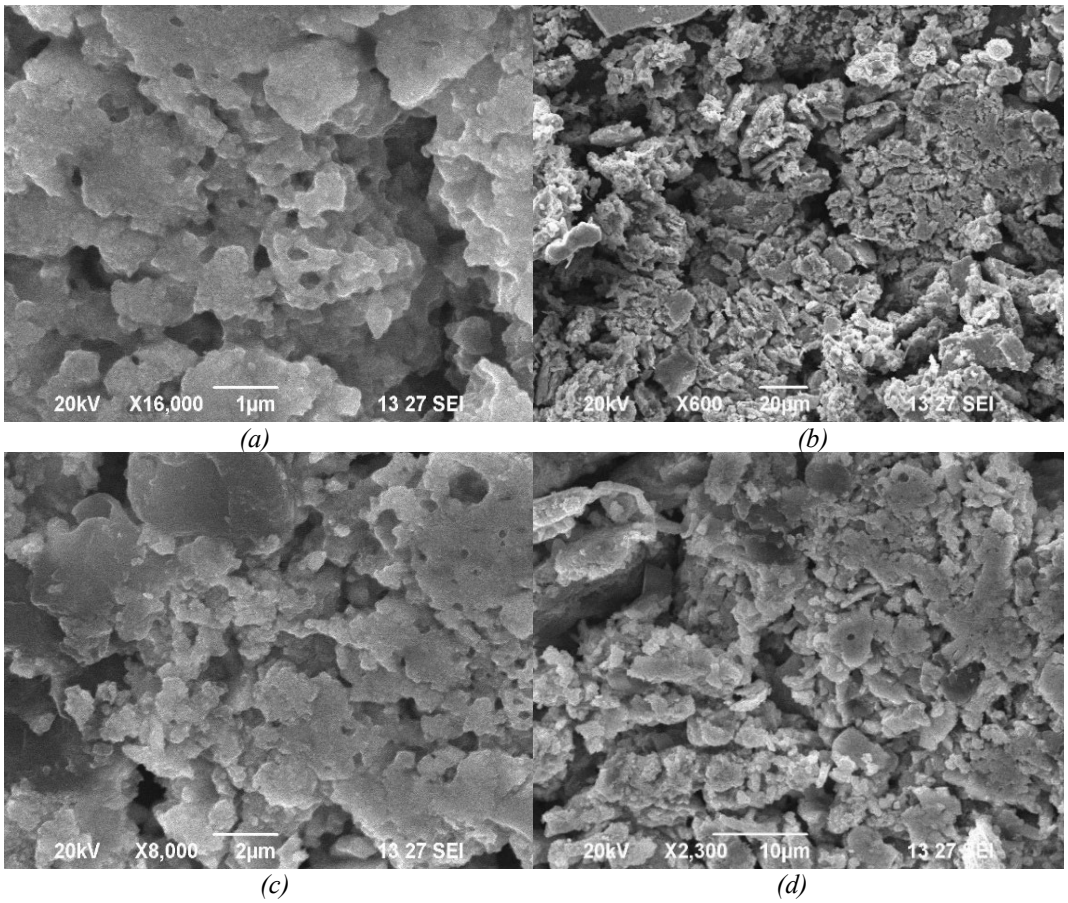

Fig. 5. (a, b, c, d) SEM Analysis of Ea-AgNPs-Si.

Figure 5 (a, b, c, d) provides an insightful view of the surface morphology, size and shape of the nanocomposite, which were examined using a Scanning Electron Microscope (SEM). The primary shape observed is predominantly flower like is attributed to the presence of phytochemicals, while several aggregates lacking a specific shape likely a consequence of secondary metabolites found within the leaf extracts. Notably, the SEM image reveals that the size of the composite falls within the range of 100 nm. The EDX analysis further substantiated the presence of a discernible peak within the silver and silica spectrum, thereby affirming the formation of nanocomposite, as delineated in Figure 6. Notably, the optical absorption peak, resonating at an approximate energy level of 1.60 &3 keV, is emblematic of the characteristic absorption pattern associated with silica and silver nanoparticles attributed to surface plasmon resonance. Worth highlighting is the conspicuous absence of any extraneous peaks in EDX, thereby ascertains the highest purity of the resultant silver nanoparticles encapsulated in silica.

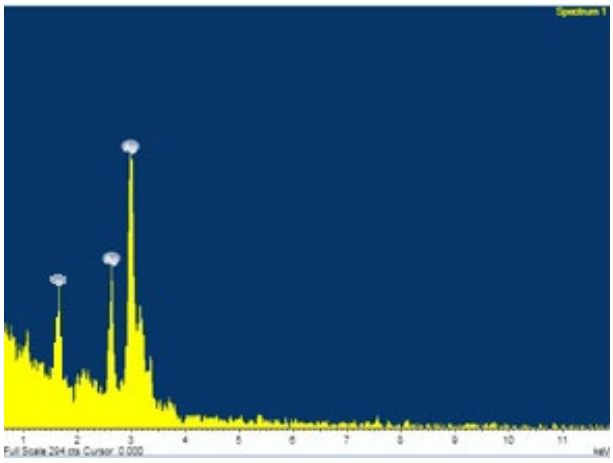

Fig. 6. EDX Analysis of Ea-AgNPs-Si.

3.2. Poultry reformer

Report says that [62] 70% of ammonia is emitted from livestock manure as ammonium($NH4^{+}$) which is then converted to ammonia (NH3) through volatilization .While the livestock manure in liquid form (slurry) used as artificial fertilizer emits 66% of ammonia which is locked up in terrestrial and aquatic ecosystem by runoff water leads to eutrophication and acidification, where ammonia is converted to nitrate by bacteria (eqn.1 & 2).These were the major contribution while 15%, 10%, 4% from ocean, wild fire and industrial process. High level of ammonia exposure may lead to liver disorder, hepatic encephalopathy, Reye's syndrome, chickenpox, renal failure, haemolytic disease etc.

$$NH3(aq) + O2(g) \text{ ----- } NO2\text{-}(aq) + 3H + (aq) + 2e - \quad (1)$$

$$NO2\text{-}(aq) + H2O\ (l) \text{ ----}NO3\text{-}\ (aq) + 2H + (aq) + 2e - \quad (2)$$

The presence of LA in water is confirmed by titrating it with 1N hydrochloric acid with methyl red indicator. The total distilled liquid is 12 mL. From that 10 mL of the LA is pipetted out and mixed with 990 mL of distilled water to make 10 ppm solution. This weak base solution is utilised for further studies. The obtained LA is colourless and was with characteristic pungent odour. The pH of the solution varies from 11.2 to 12.7. Ea-AgNPs-Si, is a highly porous material with a large surface area, which makes it effective for adsorbing LA. The adsorption process typically occurs through physical adsorption, where LA is attracted to and adhere to the surface of the silica and silver particles due to van der Waals forces. In addition, Ea-AgNPs-Si with a well-defined pore structure enhances adsorption by providing channels for LA to access the surface. Also surface functional groups on Ea-AgNPs-Si, such as hydroxyl (-OH) groups, interact with, facilitating adsorption. Higher temperatures and lower pressures typically decrease adsorption capacity.

Table 2. Experimental statistics for adsorption of LA(I), (II), (III) using Ea-AgNPs -Si composite.

Variables	Range	Maximum Percentage Removal (%)			Equilibrium Parameters		
		LA (I)	LA(II)	LA (III)	LA (I)	LA(II)	LA(III)
Initial LA Concentration (mg/L)	0.005-0.1	98.27	94.55	95.34	0.07	0.08	0.08
Adsorbent Dosage (g)	0.5-6	95.30	97.89	95.30	3.5	4.5	5.5
Initial pH	1-12	98.08	92.35	90.25	8	8	8
Contact Time (min)	10-120	97.45	93.45	92.00	50	70	90
Agitation Speed (rpm)	50-500	96.02	91.45	93.65	250	350	400

Table 2 illustrates the adsorption performance of the Ea-AgNPs-Si composite for LA (I), LA(II) and LA(III) at different initial concentrations. The composite displayed higher adsorption capacity at lower concentrations due to increased collision efficiency between LA ions and the adsorbent. However, as concentrations rise, adsorption efficiency declined likely due to limited binding sites. The hierarchy of adsorption affinity was LA (I) > LA(II) > LA(III). Near-complete saturation occurred at approximately 0.07 mg/L for LA (I) and 0.08 mg/L for LA(II) and LA(III). pH significantly influenced LA adsorption, with optimal efficiency observed at pH 7-8. The increasing adsorbent quantity from 0.5 grams to 6 grams enhanced LA removal efficiency, peaking at 95.30%, 97.89% and 95.30% for LA (I), LA(II) and LA(III), respectively. Equilibrium was reached between 3.5 g to 5.5 g. Studying different contact times revealed rapid adsorption between 50 to 90 minutes, with efficiency plateauing thereafter. Beyond 90 minutes, removal efficiency decreased, indicating time as a significant factor in adsorption.

Table 3. Adsorption isotherm parameters for LA (I), LA(II), LA(III) using Ea-AgNPs-Si.

S. No.	Adsorption Isotherm	Parameters	Equilibrium Isotherm		
			LA (I)	LA(II)	LA(III)
1	Freundlich	n	8.01	8.38	9.04
		K_F (L/g)	0.8164	0.89	0.9913
		R^2	0.5865	0.5996	0.5433
2	Langmuir	K_L (L/mg)	0.8017	0.8526	0.952
		R_L	0.0048	0.0059	0.0055
		R^2	0.9972	0.9461	0.916
3	Tempkin	A	1.918	1.40	1.06
		B	0.025	0.025	0.025
		R^2	0.8064	0.7064	0.8719
4	BET	R^2	0.799	0.695	0.694
		Surface Area (m^2/g)	300	280	220
		Pore size (nm)	29.048	25.04	23.05
5	Pseudo I order	R^2	0.7117	0.8551	0.7201
6	Pseudo II order	R^2	0.9827	0.9455	0.9534

To ascertain the adsorption characteristics of LA (I), LA(II) and LA(III), onto Ea-AgNPs-Si composite, we subjected the experimental data to rigorous scrutiny using the Freundlich, Langmuir, Tempkin Isotherm, BET models Pseudo I and II order reactions (Figure 9a-e). In Table 3, the parameters extracted from these diverse models furnish critical insights into the adsorbent's surface properties and its propensity to attract the adsorbates. It is unequivocally evident from the data that the Langmuir isotherm and Pseudo II order reaction provides a superior fit compared to the Freundlich isotherm, Tempkin isotherm and BET models. This observation underscores the presence of a monolayer chemisorption. The correlation coefficient (R^2) values, approaching 0.9972, 0.9461, 0.916, 0.9827, 0.9455 and 0.9534 for LA (I), LA(II) and LA(III), respectively, affirm the appropriateness of Langmuir and Pseudo II order model. Moreover, our choice of the Langmuir model gains further validation through the examination of the dimensionless separation factor (RL). With RL values ranging from 0.0048 to 0.0059 for LA (I), LA(II) and 0.0055 for LA(III), all falling within the coveted interval between 0 and 1, it becomes abundantly clear that the adsorption process is indeed favourable and conforms to monolayer chemisorption dynamics.

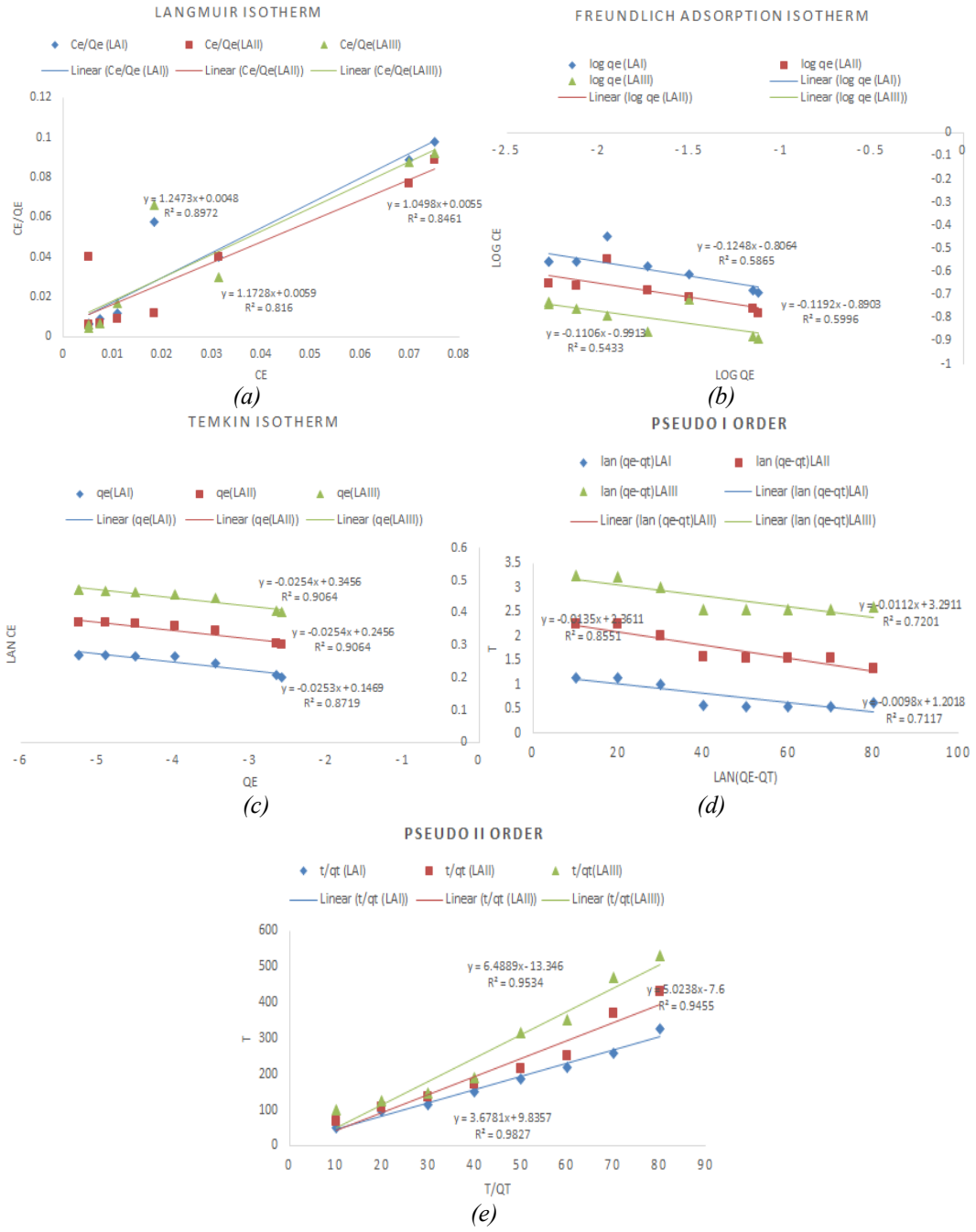

Fig. 9. (a) Langmuir Isotherm; (b) Freundlich Isotherm; (c) Temkin Isotherm; (d) Pseudo I Order; (e) Pseudo II Order

An artificial neural network (ANN) model was developed to predict the removal efficiency of LA (I), LA (II), LA (III) from aqueous solution using R2011a Matlab neuro solution to validate the above experimental batch. The model used a single hidden layer multilayer perceptron (MLP) trained with backpropagation (BP) and Levenberg-Marquardt (LM) algorithms. Input comprised five neurons (pH, adsorbent dosage, initial concentration, agitation, contact time); output consisted of three neurons for LA removal efficiency.The optimal number of hidden nodes was determined to be 5 based on minimizing mean square error (MSE). Regression analysis demonstrated a high correlation coefficient of R=0.9998(fig)with best validation at poch number 5(Figure 10a-b) and it's worth proving that while Ea-AgNPs-Si can effectively adsorb LA. The desorption of the adsorbed molecules is possible by heating, allowing for regeneration of the Ea-AgNPs-Si material for further

use. Additionally, Standard Operating Procedures (SOPs) are imbibed while handling ammonia, in order to prevent hazardousness. This study confirms that LA(basic) gets tightly bound to surface of Ea-AgNPs-Si due to its acidic nature. Hence this adsorbent is promising in the removal of ammonia from poultry which is a pollutant.

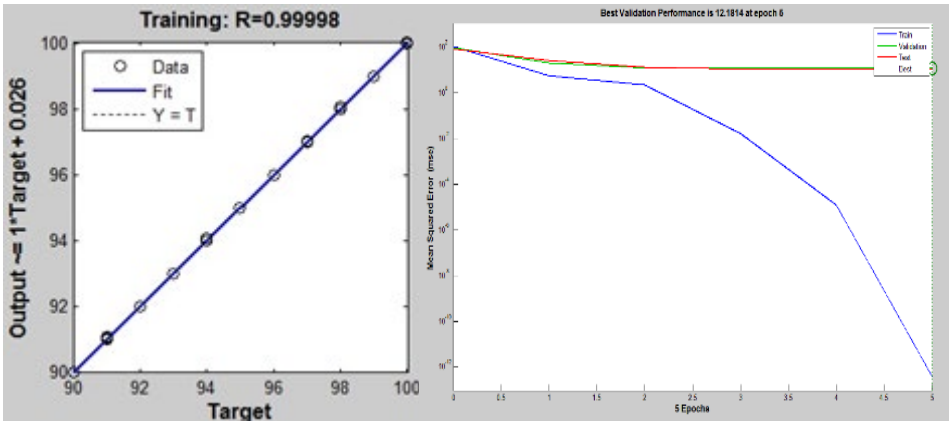

(a) *(b)*

Fig. 10. (a) Prediction of adsorption using ANN; (b) Best validation performance with least MSE.

3.3. Electrophoretic mobility

The Ea-AgNPs-Si composite's surface charge, depicted as -1.24 mV in Figure 10, correlates with its colloidal stability by repelling silver nanoparticles to prevent agglomeration. The composite also showed a polydispersity index (PDI) of 1, typical for silver nanoparticles, where 0 indicates monodisperse distribution [33], indicating polydisperse characteristics in this study.

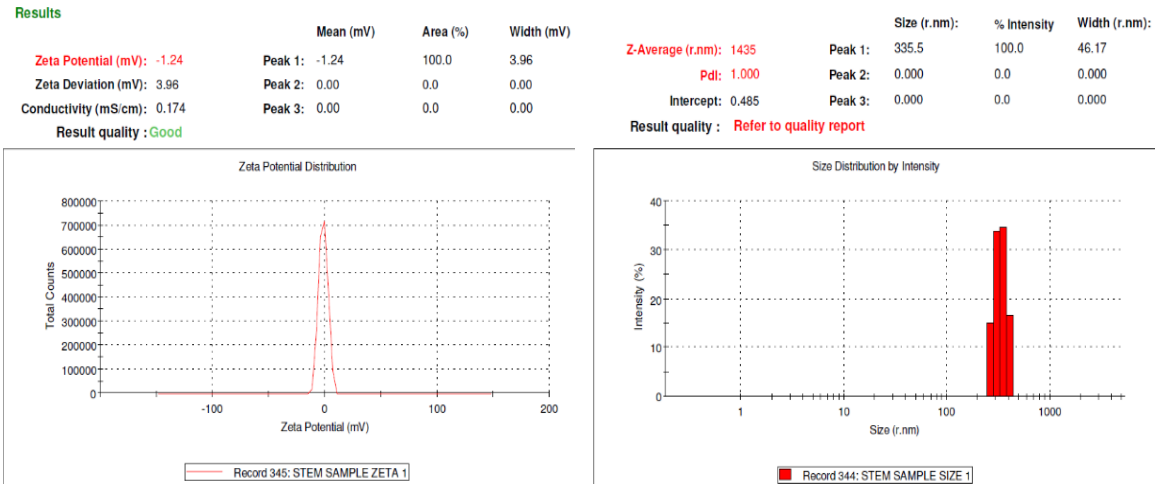

Fig. 10. Particle size distribution.

3.4. Pathogen suppressor

A larger zone of inhibition in disc diffusion method indicates that Ea-AgNPs-Si has stronger antimicrobial activity, effectively restraining the growth of Staphylococcus aureus, Actinomycetes, Escherichia coli, Klebsiella pneumonia and Pseudomonas aeruginosa. This is due to Ea-AgNPs-Si diffusing deeper into the control releasing silver ions and silica, thereby more efficiently inhibiting microbial growth by electrostatic force of attraction and affinity for silver ions. The sizes of inhibition zones are compared across various concentrations (fig:20,40,60µl) of Ea-AgNPs-Si to

assess its relative effectiveness, plates incubated at 37^0C for 24 to 48 hr (Figure 13. a-f). Higher concentrations of Ea-AgNPs-Si and longer exposure durations result in larger inhibition zones, indicating enhanced pathogen suppressor efficacy at 60 µl.

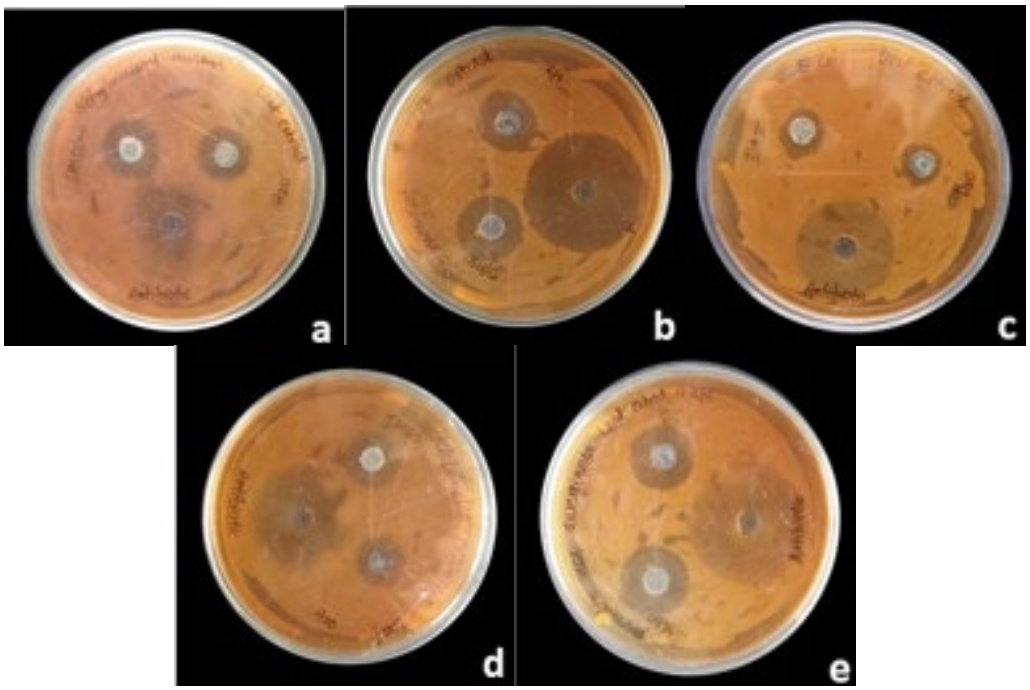

Fig. 13. (a-e) Antibacterial activity of biosynthesized Ea-AgNPs-Si for Staphylococcus aureus, Actinomycetes, Escherichia coli, Klebsiella pneumonia and Pseudomonas aeruginosa.

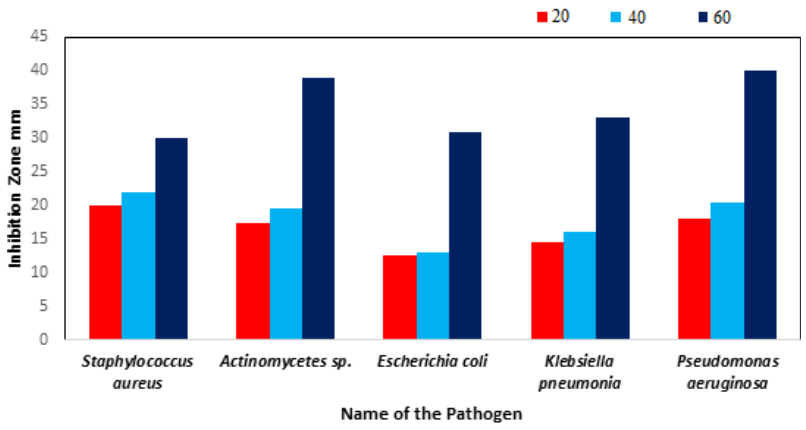

Fig. 13. f. Antibacterial activity of biosynthesized Ea-AgNPs-Si for pathogens

3.5. Sprouting catalyst

In the laboratory, we conducted a careful seed germination study, with a specific focus on the crucial role of temperature for optimal germination. We found that maintaining a temperature range of 65–70°F (18–21°C) is ideal for this purpose. The experimental setup followed a randomized design. During this investigation, we used a total of four rectangular germination trays (T1, T2, T3 and T4), each measuring 24 x 18 x 11 cm, for each population under scrutiny. These trays were filled with sand infused with Ea-AgNPs-Si. In each tray, we sowed a standardized quantity of 30 cleaned seeds of Coriandrum sativum, burying them to a uniform depth of 1 cm, resulting in a total of 120 seeds per population. To maintain appropriate moisture levels, we manually watered the sand twice

daily, ensuring continuous moisture without causing waterlogging. We began assessing germination on the 5th day after the initial seed sowing, focusing on detecting the emergence of cotyledons above the substrate surface. The results were as follows (T1=6, T2=5, T3=6 and T4=4). Throughout the experiment, we methodically recorded the number of seeds that germinated on the 10th, 15th and 20th days, (T1=10, 4, 8; T2=9, 6, 7; T3=9, 5, 8; and T4=10, 4, 8). No new seedlings emerged after the 20th day and the remaining seeds were considered dead by the 25th day. The seed count continued from the 20th day to the 25th day until no further germination events were observed. The observation period formally concluded at the end of the 25th day. Seeds that failed to germinate were systematically counted (T1=2, T2=3, T3=2 and T4=4) and a thorough physical inspection of the embryos' condition was conducted. The germination percentage for the seedlings treated with Ea-Ag-Si was calculated as follows (T1=93.33, T2=90.0, T3=93.33 and T4=86.66) using the formula GP = (TGS/TSS) x 100.We also calculated the germination value (GV) using the formula: GV = (∑DGs/N) x (GP/10). The GV for each tray was as follows (T1=1.78, T2=0.98, T3=1.96 and T4=1.2). The mean germination rate (MGR) helped us determine how quickly the seeds sprouted on average concerning the total number of seeds that sprouted each day. The MGR for trays T1, T2, T3 and T4 was 0.2, 0.1, 0.06 and 0.05, respectively. The final germination (FG) computed for T1 to T4 was 5.45. Through FG, we concluded that among the 130 seeds sown, 109 sprouted in 20 days. The germination index (GI) was used to measure how quickly and how many seeds sprouted each day, considering the time it took. Higher GI values were observed (T1=1.05, T2=1.9, T3=0.95 and T4=1.55), indicating more substantial and expedited germination. Henceforth, Ea-Ag-Si shall be employed as a nutritional catalyst to augment the proliferation of Coriandrum sativum. Ordinarily, it necessitates a span of 45 days for a single batch to attain harvest readiness; however, through our efforts, we have accomplished this feat in a mere 20 days.

4. Conclusion

This study focuses on synthesizing the nano composite Ea-AgNPs-Si from Euphorbia antisyphilitica (Ea), intending to utilize it for various purposes such as poultry reforming, acting as a sorptive material, pathogen suppressor and sprouting catalyst. Characterization techniques including XRD, SEM, TEM, Zetasizer, UV-Visible and FT-IR were employed. The synthesized Ea-AgNPs-Si exhibited a face-centered cubic arrangement with an average crystalline size of 20.34 nm. Zeta potential analysis confirmed its stability, while the PDI value indicated a polydisperse distribution. SEM imaging revealed a flower shape (Ea-AgNPs-SiO2) with diameters ranging from 70 to 100 nm.

Antimicrobial tests using the disc diffusion method showed significant activity against various pathogens attributed to its deep diffusion and silver ion release. The Langmuir isotherm and Pseudo II order model demonstrated superior fitting for monolayer chemisorption, outperforming Freundlich, Tempkin ,BET and Pseudo I order models. Additionally, final germination (FG) tests on coriander seeds indicated rapid growth with Ea-AgNPs-Si, reducing the usual 45-day growth period to just 20 days. Therefore, Ea-AgNPs-Si will be utilized as a poultry reformer, pathogen suppressor, sprouting catalyst and adsorbent.

References

[1] D. Sharma, S. Kanchi, K. Bisetty, Arabian Journal of Chemistry, 12(8), 3576(2019); https://doi.org/10.1016/j.arabjc.2015.11.002

[2] S. Iravani, R. S. Varma, Environmental Chemistry Letters, 18(3), 703(2020); https://doi.org/10.1007/s10311-020-00984-0

[3] S. M. Husseiny, T. A. Salah, H. A. Anter, Beni-Suef University Journal of Basic and Applied Sciences, 4(3), 225(2015); https://doi.org/10.1016/j.bjbas.2015.07.004

[4] R. K. Das, V. L. Pachapur, L. Lonappan, M. Naghdi, R. Pulicharla, S. Maiti, S. J. Sarma, NanoImpact, 8, 136(2017).

[5] K. S. Siddiqi, A. Husen, R. A. K. Rao, Journal of Nanobiotechnology, 16(1), 14(2018); https://doi.org/10.1186/s12951-018-0334-5
[6] J. H. Everitt, R. I. Lonard, C. R. Little, Weeds in South Texas and Northern Mexico: A Guide to Identification. Texas Tech University Press (2007).
[7] W. C. Martin, C. R. Hutchins, A Flora of New Mexico. J. Cramer 1, (1980).
[8] A. M. Powell, A. M. Powell, D. B. Wagner, Trees and Shrubs of the Trans-Pecos and Adjacent Areas. University of Texas Press. (1993).
[9] A. Singh, S. Duggal, T. Sinha, Oriental Pharmacy and Experimental Medicine, 16(2), 91(2016).
[10] L. Hartman, D. Kester, Plant Propagation: Principles and Practices. Prentice-Hal (1983).
[11] V. P. Manjamadha, K. Muthukumar, Bioprocess Biosyst Eng., 39, 401(2016); https://doi.org/10.1007/s00449-015-1523-3
[12] M. K. Swamy, K. M. Sudipta, K. Jayanta, S. Balasubramanya, Appl Nanosci., 5, 73(2015); https://doi.org/10.1007/s13204-014-0293-6
[13] V. Kumar, D. K. Singh, S. Mohan, S. H. Hasan, J Photochem Photobiol B. 55, 39(2015).
[14] B. Ajitha, Y. A. K. Reddy, P. S. Reddy, J Photoch Photobio B., 146:1(2015); https://doi.org/10.1016/j.jphotobiol.2015.02.017
[15] M. Vennila, N. Prabha, Int J ChemTech Res., 7, 2993(2015).
[16] R. Amooaghaie, M. R. Saeri, M. Azizi, Ecotoxicol Environ Saf., 120, 400(2015); https://doi.org/10.1016/j.ecoenv.2015.06.025
[17] D. K. Verma, S. H. Hasan, R. M. Banik, J Photochem Photobiol B., 155, 51 (2016); https://doi.org/10.1016/j.jphotobiol.2015.12.008
[18] K. Kamachandran, D. Kalpana, Y. Sathishkumar, Y. S. Lee, K. Ravichandran, G. G. Kumar, J Ind Eng Chem., 35, 29(2015); https://doi.org/10.1016/j.jiec.2015.10.033
[19] P. Tippayawat, N. Phromviyo, P. Boueroy, A. Chompoosor, Peer J., 4, 2589(2016); https://doi.org/10.7717/peerj.2589
[20] M. Ali, B. Kim, K. D. Belfeld, D. Norman, M. Brennan, G. S. Ali, Mat Sci Eng C., 58, 359(2016); https://doi.org/10.1016/j.msec.2015.08.045
[21] M. Govindarajan, M. Rajeswary, K. Veerakumar, U. Muthukumaran, S. L. Hoti, H. Mehlhorn, D. R. Barnard, G. Benell, Parasitol Res., 115, 723(2016); https://doi.org/10.1007/s00436-015-4794-3
[22] C. Panneerselvam, K. Murugan, M. Roni, A. T. Aziz, U. Suresh, R. Rajaganesh, P. Madhiyazhagan, J. Subramaniam, D. Dinesh, M. Nicoletti, A. Higuchi, A. A. Alarfaj, M. A. Munusamy, S. Kumar, N. Desneux, G. Benelli, Parasitol Res., 115, 997(2016); https://doi.org/10.1007/s00436-015-4828-x
[23] R. Karthik, Y. Hou, S. Chen, A. Elangovan, M. Ganesan, J Ind Eng Chem., 37, 330(2016); https://doi.org/10.1016/j.jiec.2016.03.044
[24] S. Sedaghat, A. E. Agbolag, S. Bagheriyan, J Nanostrut Chem., 6, 25(2016); https://doi.org/10.1007/s40097-015-0176-8
[25] S. Ahmed, M. Saifullah Ahmad, B. L. Swami, S. Ikram, J Rad Res Appl Sci., 9, 1(2016); https://doi.org/10.1016/j.jrras.2015.06.006
[26] M. Latha, M. Priyanka, P. Rajasekar, R. Manikandan, N. M. Prabhu, Microb Pathog., 93, 88(2016); https://doi.org/10.1016/j.micpath.2016.01.013
[27] B. Paul, B. Bhuyan, D. D. Purkayastha, S. S. Dhar, J Photochem Photobiol B., 154, 1(2016); https://doi.org/10.1016/j.jphotobiol.2015.11.004
[28] C. Shanmugam, G. Sivasubramanian, B. K. Parthasarathi, K. Baskaran, R. Balachander V. R. Parameswaran, Appl Nanosci., 6, 711(2016); https://doi.org/10.1007/s13204-015-0477-8
[29] I. M. El-Sherbiny, A. El-Shibiny, E. Salih E, J Photochem Photobiol B., 160, 355(2016); https://doi.org/10.1016/j.jphotobiol.2016.04.029

[30] A. Sengottaiyan, R. Mythili, T. Selvankumar, A. Aravinthan, S. Kamala-Kannan, K. Manoharan, P. Thiyagarajan, M. Govarthanan, J. Kim, Res Chem Intermed, 42, 3095(2016); https://doi.org/10.1007/s11164-015-2199-7

[31] M. Harshiny, M. Matheswaran, G. Arthanareeswaran, S. Kumaran, S. Rajasree, Ecotoxicol Environ Saf., 121, 135(2015); https://doi.org/10.1016/j.ecoenv.2015.04.041

[32] H. Kolya, P. Maiti, A. Pandey, T. Tripathy, J Anal Sci Technol., 6, 33(2015); https://doi.org/10.1186/s40543-015-0074-1

[33] A. R. Allafchian, S. Z. Mirahmadi-Zare, S. A. H. Jalali, S. S. Hashemi, M. R. Vahabi, J Nanostruct Chem., 6, 129(2016); https://doi.org/10.1007/s40097-016-0187-0

[34] K. Ali, B. Ahmed, S. Dwivedi, Q. Saquib, A. A. Al-khedhairy, J. Musarrat, PLoS ONE., 10, e0131178(2015); https://doi.org/10.1371/journal.pone.0131178

[35] T. A. Devi, N. Ananthi, T. P. Amaladhas, J Nanostruture Chem., 6, 75(2016); https://doi.org/10.1007/s40097-015-0180-z

[36] A. Devadiga, K. V. Shetty, M. B. Saidutta, Int Nano Lett., 5, 205(2015); https://doi.org/10.1007/s40089-015-0157-4

[37] T. Sowmyyan, G. V. Lakshmi, World J Pharm Pharm Sci., 5, 786(2015).

[38] B. Sundararajan, G. Mahendran, R. Thamaraiselvi, B. D. Ranjitha Kumari, Mater Sci., 39, 423(2015); https://doi.org/10.1007/s12034-016-1174-2

[39] K. Jadhav, D. Dhamecha, D. Bhattacharya M. Patil, J Photochem Photobiol B., 155, 109(2016); https://doi.org/10.1016/j.jphotobiol.2016.01.002

[40] R. Kanchana, P. Zantye, Asian J Pharm Clin Res., 9, 1124(2016).

[41] D. Singh, D. Rawat, B. Isha, Bioresour Bioprocess., 3, 14(2016); https://doi.org/10.1186/s40643-016-0090-z

[42] D. Bose, S. Chatterjee, Appl Nanosci., 6, 895(2016); https://doi.org/10.1007/s13204-015-0496-5

[43] M. A. Awad, W. K. Mekhamer, N. M. Merghani, A. A. Hendi, K. M. O. Ortashi, F. Al-Abbas, N. E. Eisa, J Nanomater., 943821, 6(2015).

[44] M. J. Ahmed, G. Murtaza, A. Mehmood, T. M. Bhatti, Mater Lett. 153, 10(2015); https://doi.org/10.1016/j.matlet.2015.03.143

[45] K. Elangovan, D. Elumalai, S. Anupriya, R. Shenbhagaramam, P. K. Kaleena, K. Murugesan, J Photochem Photobiol, B., 151, 118(2015); https://doi.org/10.1016/j.jphotobiol.2015.05.015

[46] S. G. Ali, H. M. Khan, M. Jalal, M. A. Ansari, A. A. Mahdi, M. K. Ahmad, Asian J Pharma Clin Res., 8, 335(2015).

[47] M. Parveen, F. Ahmad, A. M. Malla, S. Azaza, Appl Nanosci., 6, 267(2016); https://doi.org/10.1007/s13204-015-0433-7

[48] R. S. Priya, D. Geetha, P. S. Ramesh, Ecotoxicol Environ Saf., 134, 308(2015); https://doi.org/10.1016/j.ecoenv.2015.07.037

[49] K. Murugan, M. A. Labeeba, C. Panneerselvam, D. Dinesh, U. Suresh, J. Subramaniam, P. Madhiyazhagan, J. Hwang, L. Wang, M. Nicoletti, G. Benelli, Res Vet Sci., 102, 127(2015); https://doi.org/10.1016/j.rvsc.2015.08.001

[50] U. Muthukumaran, M. Govindarajan, M. Rajeswary, Parasitol Res., 114, 4385(2014); https://doi.org/10.1007/s00436-015-4677-7

[51] M. Govindarajan, M. Rajeswary, K. Veerakumar, K. Muthukumaran, S. L. Hoti, G. Benelli, Exp Parasitol., 161, 40(2016); https://doi.org/10.1016/j.exppara.2015.12.011

[52] M. Sigamioney, S. Shaik, P. Govender, S. B. N. Krishna, Sershen, Mart. Ex Thell S Afr J Bot., 103, 230(2016); https://doi.org/10.1016/j.sajb.2015.08.022

[53] A. Varghese, P. Anandhi, R. Arunadevi, A. Boovisha, A, Sounthari, J. Saranya, K. Parameswari, S. Chitra, JPSR., 7, 266(2015).

[54] S. Perugu, V. Nagati, M. Bhanoori, Appl Nanosci., 6, 747(2016); https://doi.org/10.1007/s13204-015-0486-7

[55] K. Anandalakshmi, J. Venugobal, V. Ramasamy, Appl Nanosci., 6, 399(2016); https://doi.org/10.1007/s13204-015-0449-z
[56] K. Arunachalam, B. Shanmuganathan, P. S. Sreeja, T. Parimelazhagan, Environ Sci Pollut Res., 22, 18066(2015); https://doi.org/10.1007/s11356-015-4992-7
[57] B. Srinithya, V. V. Kumar, V. Vadivel, B. Pemaiah, S. P. Anthony, M. S. Muthuraman, Mater Lett., 170, 101(2016); https://doi.org/10.1016/j.matlet.2016.02.019
[58] R. Sriranjani, B. Srinthiya, V. Vadivel, B. Pemaiah, S. P. Anthony, A. Sivasubramanian, M. S. Muthuraman, J Mol Liq., 220, 926(2016); https://doi.org/10.1016/j.molliq.2016.05.042
[59] S. Muthukrishnan, S. Bhakya, T. Senthil Kumar, Ind Crop Prod., 63, 119(2015); https://doi.org/10.1016/j.indcrop.2014.10.022
[60] K. L. Niraimathi, V. Sudha, R. Lavanya, P. Brindha, Coll Surf B Biointerface., 102, 288 (2013); https://doi.org/10.1016/j.colsurfb.2012.08.041
[61] H. Esechie, J. Agron. Crop Sci., 172, 194(1994); https://doi.org/10.1111/j.1439-037X.1994.tb00166.x
[62] W.A.H. Asman, M.A. Sutton, J.K. Schjoerring, New Phytol., 139(1), 27(1998); https://doi.org/10.1046/j.1469-8137.1998.00180.x